sustainability

MDPI

Article

Response of Organic Lime Mortars to Thermal and Electrical Shocks Due to Lightning Strikes

Thirumalini Selvaraj [1,*], Venkatesh Srinivasan [2], Simona Raneri [3], Manjula Fernando [4], Kunal Kakria [1] and Simon Jayasingh [1]

[1] School of Civil Engineering, Vellore Institute of Technology, Vellore 632014, India; Kunalkakria@yahoo.com (K.K.); simon.jayasingh@vit.ac.in (S.J.)
[2] School of Electrical Engineering, Vellore Institute of Technology, Vellore 632014, India; venkatesh.srinivasan@vit.ac.in
[3] Italian National Research Council, ICCOM-CNR, 56124 Pisa, Italy; simona.raneri@pi.iccom.cnr.it
[4] Department of Electrical & Electronic Engineering, University of Peradeniya, Peradeniya 20400, Sri Lanka; manjula@ee.pdn.ac.lk
* Correspondence: thirumalini.selvaraj@vit.ac.in

Received: 30 June 2020; Accepted: 30 August 2020; Published: 2 September 2020

Abstract: Lightning strikes are prevalent and inevitable natural phenomena that might cause damages during interaction with building structures and, in some cases, culminate in fires. During the last decades, several lightning strikes have caused considerable damages to cultural and heritage buildings. Furthermore, recent studies indicated a plausible connection between climate changes due to global warming and variations in the frequency and intensity of lightning. The evaluation of the structural efficiency and resilience of cultural buildings to global changes and natural risks appears significant in the light of the current scientific debate. This research aims at the assessment of lightning strikes' effects on ancient heritage binding materials through the characterization of their thermal and electrical conductivity properties. This study focused on the performance evaluation of green and low-cost mortars based on the use of organic additives. Lime samples were reverse engineered by using a mixture of organics (fig, jaggery, black grape, banana, kadukai), which comprises the most common additives used in traditional Indian mortars. The reliability of the organic mixture in enhancing the resilience of masonry to lightning strikes was analyzed by using electromagnetic field simulation.

Keywords: lightning strikes; lime mortars; organic additives; resilience; sustainable repair materials

1. Introduction

Heritage monuments and buildings are structures possessing architectural splendor, aesthetics, elegance, historic significance, and cultural values [1]. The protection of cultural buildings from natural and environmental risks represents a big challenge; adverse weather and climate, pollution, and uncontrolled urbanization are only few of the risks to which cultural buildings are exposed [2]. Natural disasters, such as lightning strikes, floods, earthquakes, fires, environmental fatigues or similar long-term climate effects can cause irreversible damage to cultural heritage or destroy entire areas of cultural value, involving both movable and immovable art objects [3]. Recently, an increasing number of lightning strikes on heritage monuments have been reported in India, probably more than elsewhere in the world [4]. Table 1 summarizes a few significant lightning strikes recorded in the last decade at important monuments and buildings around the world [5].

Table 1. Lightning strikes at major heritage structures worldwide [5].

Name of the Monument	Location	Year of Lightning Strike	Damage to the Monument
Parthenin Temple	Athens, Greece	June 2010	Impairments to structures
Statue of Liberty	New York, US	October 2010	Reported to have been hit by hundreds of strikes since 1886
Big Temple	Thanjavur, India	November 2010	Broken Kalash (spire or sacred vessel) on Rajajrajan Tower (Thiruvayil or gopuram) top
Pratapur Temple	Kathmandu Valley, Nepal	February 2011	Stairway to south side entrance debilitated with one sculpture dislocated
Eiffel Tower	Paris, France	July 2012	No major damage reported
Sigiriya Rock Fortress	Dambulla, Sri Lanka	October 2012	One of Lion's paws at entrance damaged
St. Peter's Dome	Vatican City, Holy See	February 2013	No major damage reported
World Trade Centre	New York, US	September 2013	No major damage reported
Sri Meenakshi Amman Temple	Meenakshi, India	December 2013	East Rajagopuram damaged
Tower Bridge	London	January 2014	Train services suspended
Christ- The Redeemer Statue	Rio de Janeiro, Brazil	January 2014	The middle finger of the right-hand got chipped
Sydney Opera House	Sydney, Australia	April 2014	Defaced with fine cracks
CN tower	Canada	June 2015	No major damage reported
Golden Gate Bridge	California, US	November 2015	No damage to the structure but reported power-cut in adjoining areas
Angel Moroni Statue-Bountiful Utah Temple	USA	May 2016	Damage to the head and back of the statue
Jameshwar Temple	Bhubaneswar, India	July 2016	A deep crack developed in walls
The Washington Monument	Washington D.C., US	July 2016	Aluminium pyramidion melted due to repeated strikes

Figure 1 depicts snapshots of the damages caused to some important United Nations Educational, Scientific, and Cultural Organization (UNESCO) world heritage monuments that have been struck by lightning in India. In Brihadisvara Temple (Big Temple), in Thanjavur, one of the five spires (called kalasam) atop the Rajarajan gopuram (called also Thiruvayil), which is the middle gopuram from the entrance of the temple (Figure 1a) was damaged by a lightning strike [6]; the kalasam made of brick and lime mortar fell and broke into several pieces. Another example is the Jameshwar Temple (Bhubaneshwar) (Figure 1b), which experienced extensive damages from a lightning strike that caused a deep crack on the 11th-century temple's wall on its exterior ornament [7]. In 2013, a lightning strike hit the Ratneswhwar Mahadev temple in Varanasi [8] (Figure 1c), which was extensively damaged and required a significant refurbishment. The Nilamadhab temple was hit by a lightning strike that caused damages to the sanctuary's spire [9] (Figure 1d). Furthermore, a lightning strike hit the famous world heritage UNESCO site of Khajuraho, damaging the top part of the Devi Jagadambika temple (Figure 1e), inside the western group of temples [10]. Another important monument, the Charminar, was recently hit by a lightning strike. It was reported that the building was damaged several times by lightning strikes on its south-western minaret [11]. Reports have also mentioned that one of the 35 m high bell tower of the Se Cathedral (Goa) was extensively damaged by a lightning strike in 1776 (Figure 1f) [12].

(**a**)

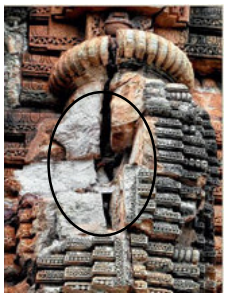

(**b**)

(**c**)

(**d**) (**e**) (**f**)

Figure 1. Lightning strikes on heritage sites in India: (**a**) Brihadisvara Temple, (**b**) Jameshwar Temple, (**c**) Ratneshwar Mahadev Temple, (**d**) Nilamadhab Temple, (**e**) Jagadambika Temple, (**f**) Se Cathedral. The ovals mark the structural element hit by lightning strikes and the produced damages.

The structural instability of the monuments during and after lightning is directly related to the type and nature of building materials used in construction and their resistance to the thermal and electrical energy generated from lightning [13]. Since ancient times, different kind of materials, from herbs to mud and from stone and blocks to metals have been used in construction work [14]. Ancient materials used in heritage structures were usually designed to improve the resilience of the structure in respect to local weather conditions [15]. In India, a country that experiences six different climatic conditions, the construction materials and production technologies are region-specific and based on the availability of local raw materials [16]. Till the 19th century, lime-based mortars became predominant in construction work; with the advent of Portland cement, the use of lime mortar slowly disappeared from the construction, due to its inferior properties relative to cement. However, cement is incompatible with ancient materials, thus necessitating the design and the optimization of appropriate repair materials for the conservation and restoration of heritage buildings [17–20]. In India it has been a common practice to add organics to lime; this feature has been utilized to improve the hardening properties of lime mortars [16,21].

The focus of this research was the assessment of the role of organics in modifying the thermal and electrical properties of lime-based mortars to better understand its efficiency in heritage monuments. Reverse-engineered lime-based organic mortars were formulated and their electrical and thermal conductivity characteristics were studied, along with their mechanical properties. Additionally, thermal and electrical properties were evaluated in samples from ancient heritage buildings for which a higher resilience concerning lightning strikes has been observed over time. Finally, in this paper a detailed electrical simulation and analysis are proposed in order to evaluate the reliability of organic mortars in improving the resilience of heritage buildings to lighting strikes.

2. Lightning Parameters—Insights into Structural Aspects and Requirements

2.1. General Aspects of Lightning Parameters

Lightning can be categorized into four types, namely negative cloud-to-ground (−CG), positive cloud to ground (+CG), positive ground to cloud (+GC), and negative ground-to-cloud (−GC), as illustrated in Figure 2. Among these, the positive cloud-to-ground (+CG) type is five to six times more powerful than the others, which can in turn cause extensive damage to structures [22,23]. Such severe lighting strikes due to +CG occur in stratified squall-line regions of thunderstorms, while the −CG lightning strikes are most common and occur during the monsoon. The upward-directed +GC and −GC occur invariably in very tall structures.

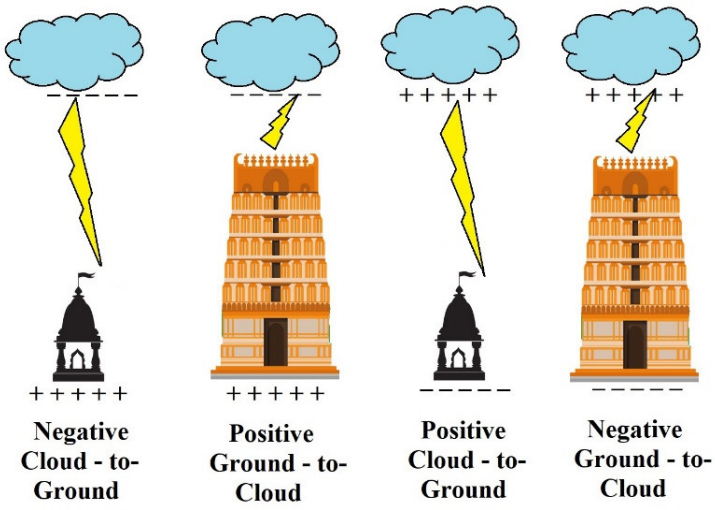

Figure 2. Types of lightning strikes.

CG lightning strikes can transfer energy in the range of 100–1100 J, wherein this energy is invariably converted into producing thunder, hot air, light, and radio waves. In such cases, lightning may reach a speed of 94 km/s. The maximum temperature in the channel during lightning is in the range of 10,000–30,000 K. Furthermore, when CG lightning strikes materials such as soil, rock, clay, etc., the stroke current flows through the material, heating it and in some cases reaching the vaporization point, with a consequent sudden cooling (quenching). This may lead to changes in the morphological structure of materials. Detailed studies on the energy released by lightning strikes reported that CG lightning may release about 6 MJ/m, which leads to the dissociation of materials such as rocks [24].

Figure 3 depicts the development of return stroke current on a grounded structure (considered to be a conductor) during a lightning strike and the resulting radiated magnetic field during the initiation of the return stroke, which develops within a few tens of microseconds. The nature of the upward-directed return stroke that is initiated during lightning is invariably along a vertical channel profile.

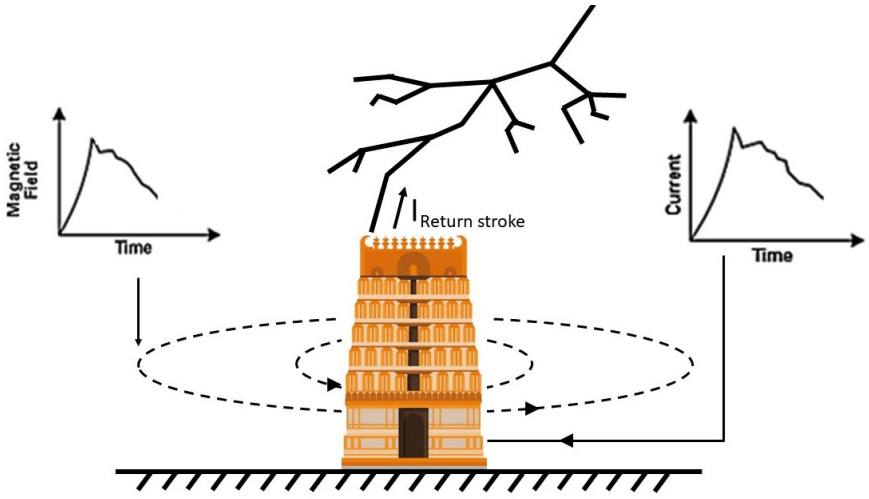

Figure 3. Pictorial representation of radiated electromagnetic field during the development of a lightning return stroke.

Figure 4 illustrates the concept of skin effect and hence the skin depth (depth of penetration) in an electrically conductive object; it can be argued that as the frequency of the excitation increases, the skin depth (penetration depth) of the component decreases.

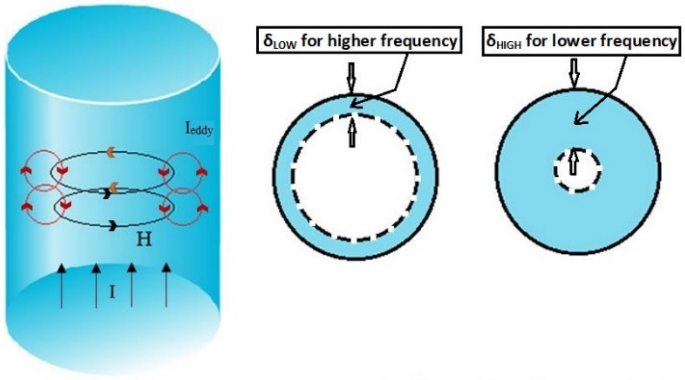

Figure 4. Generic concept of skin effect in grounded conducting structure.

As an example, an electromagnetic field simulation of a heritage building structure of a typical temple tower structure ("Keralanthakan gopuram") in Brihadesvara temple is presented in Figure 5, which illustrates the skin depth obtained during the simulation of lightning studies. The Brihadesvara temple monument is a major heritage structure in south India dated to the 10th century and made of granite stone; in recent times, it was hit by lightning strikes on its towers (called "gopurams").

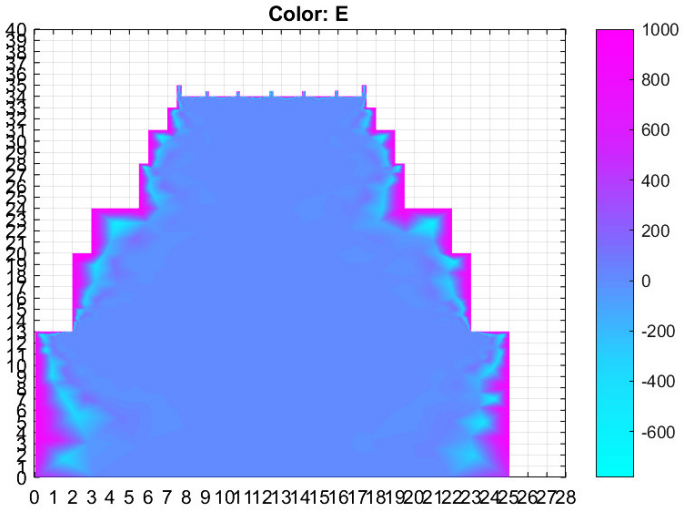

Figure 5. Simulation of skin effect for a temple tower (Gopuram) structure (Drawn to Scale 1:1 m).

The electrical parameters used for the modeling and the simulation of the structure during lightning strikes are the following: σ (electrical conductivity) = 1 mS/m; ε_r (dielectric permittivity) = 6 and magnetic permeability = 16; frequency = 10 kHz. The 2-dimensional geometrical model of the structure is drawn with the scale in meters (m) and the output is shown as a color plot that represents the variations in electric field intensity (E) at the chosen frequency (f). The highest magnitude of electric field intensity is shown in pink and minimum magnitude of the electric field is shown in blue.

The adverse impacts of lightning strikes on different construction materials utilized in structures, buildings, and landmarks (such as concrete, stone, wood, and steel) would have considerable variations; moreover, the location and the distribution of possible metallic constituents in a building can contribute to the granular disintegration of the structure. Lightning strikes on buildings can cause cracks in architectural contours, which in turn diminishes their mechanical quality. They may, therefore, be responsible for secondary damages, inducing fell impacts, destruction of icons, distortion of paintings, decay of connection elements, etc. [5].

2.2. Lightning Protection of Heritage Structures—Skin Effect and Its Role on Electrical and Thermal Conductivity

The structural requirements for protecting buildings from lightning strikes are summarized in IEC 62305-3:2010 recommendation [25]. This standard extensively deliberates on the role played by material properties, such as resistive (ohmic) heating, electro-dynamic forces, and thermal and mechanical properties, in the effects of lightning strikes on buildings. Further significant parameters also include the skin effect (i.e., the skin depth δ), the frequency spectrum of the lightning wave (f), the material resistance (R), etc.

Return stroke models enable the simulation of the generation of electromagnetic fields similarly to those created by natural return strokes; several lightning return stroke models have been implemented by researchers, describing the most relevant parameters and characteristics of lightning. In this regard, transmission line models, which are based on electromagnetic field analysis, have clearly established the role played by the skin effect (and hence skin depth) of the modeled structure on the propagation of transverse magnetic (TM) waves along a single conductor (in this case, the grounded structure) [26]. It is pertinent to note that the measurement and the recording of a lightning strike need to adhere to the IEC 62305-1:2010 recommendations [27]; thus, the lightning counters are usually equipped to count lightning related to standard wave-shapes (10/350 μs and 8/20 μs). Such counters are designed to count lightning strikes in the range of 20 km dependent on specific climate condition (e.g., a 10 kHz counter in temperate regions) [28,29]. Furthermore, detailed studies and analyses based on simulation indicated that the nature of the waves guided along the conductor depends on the relative size of the lightning channel radius and the electromagnetic skin depth (δ).

Such lightning models have been applied also in heritage monuments studies [30]; simulation studies have established the role played by the skin depth and the spectrum of lightning frequencies on the impact of a lightning strike on structures. Furthermore, such studies have also computed and analyzed the typical skin depth of mortars at a frequency of 10 kHz, which was observed to be about a few meters (6 to 8 m), and the resistance of the mortar slab was observed to be about a few hundred ohms.

Since the skin depth (δ) is directly related to the depth of penetration of the lightning current during a prospective strike to a heritage structure, it is evident from Equation (1) that electrical conductivity plays a vital role in evaluating its heating and thermal withstanding capability.

$$\delta = \sqrt{\frac{2\rho}{\omega\mu}}\sqrt{\sqrt{1+(\rho\omega\epsilon)^2}+\rho\omega\epsilon} \quad (1)$$

where ρ is the resistivity in Ω-m, ω indicates the angular frequency, and μ denotes the absolute permeability of the structural material (lime mortar) taken up for analysis.

At frequencies much below $\left(\frac{2}{\mu\varepsilon}\right)$, the formula gets simplified, as indicated in Equation (2).

$$\delta = \sqrt{\frac{2\rho}{\omega\mu}} \quad (2)$$

In view of the direct correlation between the electrical conductivity and the heating of structures [31,32], the analysis of thermal conductivity in construction materials presents interesting avenues for focused research related to the role of structural materials used in monuments. In respect to heritage structures, several research surveys and reports from the international agencies dealt with the thermal analysis of ancient buildings materials [33–37], with particular attention to lime mortars, which also evidence the role of reactive additives in modifying their thermal properties [34]. It is thus of interest to study the role of organics in modifying the electrical and thermal conductivity properties of building structures in view of obtaining a better understanding of their impact on building energy efficiency.

3. Materials and Methods

3.1. Lime-Based Reverse-Engineered Mortars

Samples from heritage sites across India were collected and analyzed as a reference for realizing laboratory engineered samples. Thus, the collected samples were reverse engineered; manufacturing processes and ingredients were replicated for further analysis and to prove the effectiveness of the materials used by ancient architects. The specimens taken from the heritage sites were used as a baseline for the preparation of engineered mortar samples to prepare competent mortars with improved mechanical and durability properties. Preliminary analysis carried out by the authors on historical samples evidenced the use of several plant and animal extracts [16,38–40]; among them, plant extracts, such as kadukai, jaggery, fig, banana and grapes, were usually used alone or in combination, based on local availability and traditions that are still followed in some parts of India by craftsmen. XRD, TGA and FT-IR analyses performed on historical samples enabled us to describe the role of additives in modifying the fresh and hardened properties of mortars, which in turn influence the strength and durability of the building structures [38–40]. The organics added into Indian historical mortars are rich in carbohydrates (90–95%), protein (5–10%) and fats (in small percentages), which modify the composition and the behavior of the final binding material. The addition of organic water to lime generally increases the solubility of calcium oxide in water by 84% [41], which results in higher conversion rate of calcium hydroxide (portlandite); furthermore, the fermentation of organics results in the formation of alcohol and carbon-dioxide [42]. In such systems the carbonation of calcium hydroxide particles to calcite polymorphic phases is faster than in other environments; hence the rate of precipitation of calcite is higher when using organic extracts instead of water in mortar mixes [38]. Fats and proteins contribute in improving durability by making the mortars more resistant to environmental agents [21,43,44]. Based on the above input, in the current research, similar organic mortars were prepared in line with ancient mortars used in heritage structures.

The hydrated lime used in the investigation was obtained from Pollachi, Tamil Nadu in India. The percentage retained on an 850-micron sieve was used for the study. The chemical composition of the lime was determined by following the standard recommendations of IS 6932:1973, Part I [45] and IS 6932:1973, Part V [46]; it consists of 70 to 80% of calcium oxide and 20 to 30% of clay impurities (Al_2O_3 + Fe_2O_3 + SiO_2). The lime is classified as air-lime, in accordance with the standard recommendation IS 712:1984 [47]. The consistency and workability of lime were determined as per IS 6932:1973 Part VIII [48].

Well-graded siliceous river sand, free from dust and organic matter and with a specific gravity of 2.65, was used; it was graded according to the standard recommendation of IS 2386:1963 Part I [49]. Local clay from adjacent areas traditionally used for making pottery was used. Dry solid clay was crushed through a tilting grinding machine and the residue retained on an 850-micron sieve was used for this study.

Five different organics were used for the preparation of organic mortars, namely fig, jaggery, black grape, banana, and kadukai (Figure 6, Table 2).

(**a**)

(**b**)

(**c**)

(**d**)

(**e**)

Figure 6. Organics used in mortar preparation: (**a**) fig, (**b**) jaggery, (**c**) black grape, (**d**) banana, and (**e**) kadukai.

Table 2. List of organics and their properties.

Local Name of Organics	Botanical Name of the Organics	Properties
Fig (Figure 6a)	*Ficus carica*	Contains reducing sugar in high concentration and non-reducing sugar, protein, fat, ascorbic acid, potassium, and dietary fiber.
Jaggery (Figure 6b)	*Unrefined sugar*	Contains a high amount of sucrose, calcium, magnesium, and iron; also contains reducing sugars, protein, fats, total organic, and phosphorus.
Black grape (Figure 6c)	*Vitis Vinifera*	Is rich in carbohydrates and contains sugars, organics acids, phenolic compounds, nitrogenous compounds, volatile compounds (aroma), minerals, and pectic substances.
Banana (Figure 6d)	*Musa acuminate*	There are different types of bananas; the *Musa acuminata* was used for fermentation. It is rich in potassium; it also contains calcium, sodium, manganese, carbohydrate, crude fiber, and saponins. Isoamyl acetate is a prominent compound.
Kadukai (Figure 6e)	*Terminalia chebula*	Contains high amounts of crude fiber; it also has phenols, tannins, flavones, proteins, reducing sugars, and saponins.

The selected organics were washed in running water, crushed with a grinding machine for 15 minutes and soaked in drinking water (5% in 1 L of water). The soaked organics were sealed tightly for a fermentation period of 3–7 days. The anaerobic fermentation quickens the releasing of CO_2 with the slow formation of bubbles from the bottom to the top, whose end indicates the completed fermentation of organics. After the fermentation process, the organic liquid was filtered to separate the leftover uncrushed particles and impurities. This fermented organic water was used in organic lime mortar preparation.

According to IS 6932:1973 Part VII [50], a binder to aggregate ratio of 1: 3 was used to prepare mortars. In detail, one part of hydraulic lime and three parts of fine aggregate sand sieved through 2.36 µm and mechanically ground for 30 min to reduce the particle size and for better mix with lime were mixed. During grinding, the organic water was added. For each mixture, the water/binder ratio was adjusted based on workability by a standard flow table test, according to IS 6932 (Part VIII) [48]; results are shown in Table 3. From the obtained results it can be argued that in organic mixes the water/binder ratio ranges from 0.65 to 0.55, which is credibly related to the different organic contents in the used plant extracts.

Table 3. Flow table test results.

Sample Number.	Sample Name		Water/Binder Ratio	No. of Bumps Required to Achieve 110 mm Spread
1.	Lime + Sand	Reference Mix	0.75	10
2.		Fig	0.65	9
3.		Jaggery	0.55	8
4.		Grape	0.65	9
5.		Banana	0.60	8
6.		Kadukai	0.65	9
7.	Lime + Clay	Reference Mix	0.75	10
8.		Fig	0.68	9
9.		Jaggery	0.60	8
10.		Grape	0.65	9
11.		Banana	0.65	9
12.		Kadukai	0.65	9

The mixes that passed the workability test were cast in cubes 40 × 40 × 40 mm and cylinders 100 (diameter) × 200 mm in dimension; they were then slightly pressed to remove any air bubbles and voids and released from the mold after 28 days, by following the normal rules applied to mortars.

A total of 72 samples (36 cubes + 36 cylinders) were prepared by using five organics; three samples per each organic additive and one reference mix were used for the analysis and average values were computed in the results. Cubes were used for evaluating porosity and density and then for compressive strength tests, while cylinders were used for evaluating thermal and electrical conductivity.

Curing was carried out in controlled environmental conditions (room temperature at 27 ± 2 °C and relative humidity at 65 ± 2%). For the first 7–8 days the mixtures were kept in the molds with the upper side open, thus favoring carbonation, and then removed from the molds and kept open in the ambient atmosphere.

3.2. Compressive Strength

Compressive strength was determined by applying a slow loading rate of 1 mm/min at a room temperature of 26 °C and humidity of 60% [51]. Instron® 8801 equipment (Instron Co./ Norwood, MA, USA) was used to perform the test; it consists of a minimized servo-hydraulic weariness testing framework that fulfills the complex needs of different static and dynamic testing appropriate for weakness testing and crack mechanics. The compressive strength was calculated as indicated in Equation (3).

$$\text{Compressive strength} = \frac{failure\ load\ (kN)}{Area\ (m^2)} \quad (3)$$

3.3. Porosity and Density

The bulk density was found in accordance with Rilem Technical Report 203:2016 [52]; this parameter is calculated as the ratio of the mass to its bulk volume after 28 curing days. Porosity is the fraction of the total volume of solid occupied by pores or voids; it is calculated according to Rilem TC 25:1980 [53]. Samples were dried at 103 °C for 24 h and dry weight mass was recorded (Md). Samples were then saturated under water for 24 h and then weighed again (Ms). The Archimedes weight of samples (Ma) was also measured.

$$\mathrm{D} = \frac{M_d}{(M_s - M_a)} \quad (4)$$

$$P = [\frac{(M_s - M_d)}{(M_s - M_a)}] \cdot 100 \quad (5)$$

where D = bulk density and P = porosity.

3.4. Thermal Conductivity Testing

Thermal conductivity was tested by using a KD2 Pro Analyzer® (Decagon Devices, Inc/Pullman WA, USA); the device consists of a handheld controller and sensors that can be inserted into the samples. This apparatus enables the user to either conduct tests manually or program the controller for automatic readings. To enable the measurements, cylindrical samples with different organic compositions were cast with a hole of 5 mm diameter in the center by using a ballpoint pen refill. The RK-1 Sensor® (ICT International/Armidale, Australia) was inserted into the hole and used to measure the thermal conductivity of the samples.

3.5. Electrical Conductivity Testing

The electrical conductivity of a specific material is its capacity to exchange charged particles in an electric field; hence, it is a measure of the electrical current that the material can carry. The electrical resistivity test was conducted at the Indian Institute of Technology (IIT-Madras) at the Concrete Materials Research Lab-2 by using Resipod® (Proceq SA/Schwerzenbach, Switzerland) equipment. This test is widely accepted for measuring the surface electrical resistivity of concrete as well as lime mortar. The instrument setup consists of four equally spaced electrodes that can be placed on cylindrical samples and works on the principle of Ohm's law, as shown in Equation (6); the outer two electrodes transmit currents and the inner two electrodes measure the potential difference between them [54,55]. The resistance is calculated using Equation (6) with the resistivity measured by the given Equation (7). Conductivity is the reciprocal of resistivity, as described by Equation (8).

$$V = I \cdot R \quad (6)$$

$$\rho = \frac{R \cdot A}{L} \quad (7)$$

$$\sigma = \frac{1}{\rho} \quad (8)$$

3.6. Electromagnetic Field Simulation During Lightning Strikes

Simulation studies were carried out to ascertain the role of electric conductivity and its effect on the skin depth due to varying frequencies by using Matrix Laboratory (MATLAB®) Release 2017b software (The MathWorks, Inc/ Natick, MA, USA). The Partial Differential Equation (PDE) toolbox allows drawing the geometrical layout of the building structures in conjunction with obtaining solutions to specific parameters by utilizing the built-in Finite Element Method (FEM). In this analysis, the AC power electromagnetics tool enables carrying out a 2-dimensional analysis of the skin depth. The PDE toolbox enables the user to solve and simulate the solution to complex partial differential equations for a wide range of generic engineering applications, such as electrostatics, AC electromagnetic field, generic scalar field, heat transfer, and diffusion. The PDE Toolbox, in addition, offers a facility to compute, plot, and analyze various parameters and characteristics by solving partial differential equations with relevant boundary conditions. The boundary conditions are usually of two variants, namely Dirichlet and Neumann; Dirichlet's condition ("fixed boundary condition") allows the user to specify the values that need to be taken along the boundary of the domain taken up for analysis. However, the Neumann condition allows specifying the values of parameters wherein the derivative of a solution is utilized within the boundary of the domain.

4. Results Based on Laboratory Testing and Analysis

4.1. Laboratory Samples

4.1.1. Compressive Strength

After 28 curing days, the compressive strength of the studied mixes was lower than the ones cured for 90 days. This behavior can be explained by the still ongoing portlandite to calcite reactions and the higher moisture contents at 28 curing days; under this condition, similar values were registered in the reference and organic mixes. Otherwise, after 90 curing days, both the reference mix and the organic limes showed higher strengths than the samples cured for 28 days. Moreover, the organic limes exhibited improved mechanical properties respect to the reference mixes (Figure 7). The reference limes showed a strength gain of about 1 MPa and 3.6 MPa for the lime–sand and the lime–clay mixes, respectively. The kadukai and jaggery mixes performed the best as organic mortars, gaining a strength of 2.35 MPa and 2.81 MPa for the lime–sand mix, respectively, and 4.41 MPa and 4.93 MPa for the lime–clay composition, respectively. On the contrary, among the organic limes, the lowest values were registered for the mixes with banana and fig, with values of 1.53 and 1.76 MPa in lime–sand mixes, respectively, and 3.77 MPa and 3.89 MPa in lime–clay mixes, respectively.

Overall, the maximum strength was observed in the mixtures with clay; in fact, a strength gain 2.5 times higher than that of the lime–sand mixes was observed. This behavior might be attributed to the formation of silicate-hydrated phases, which are responsible for the improved mechanical resistance.

In summary, the addition of organics led to an overall increase in the compressive strength of about 280% for lime–clay and 140% for lime–sand mixes; these results are attributable to the forced carbonation due to the interaction between lime and organics in the lime–sand mixes, and to the combination of these reactions and the hydrated phases in the lime–clay mixes. Moreover, the addition of organics increased the binding strength of lime particles, clearly indicating higher resistance to compression.

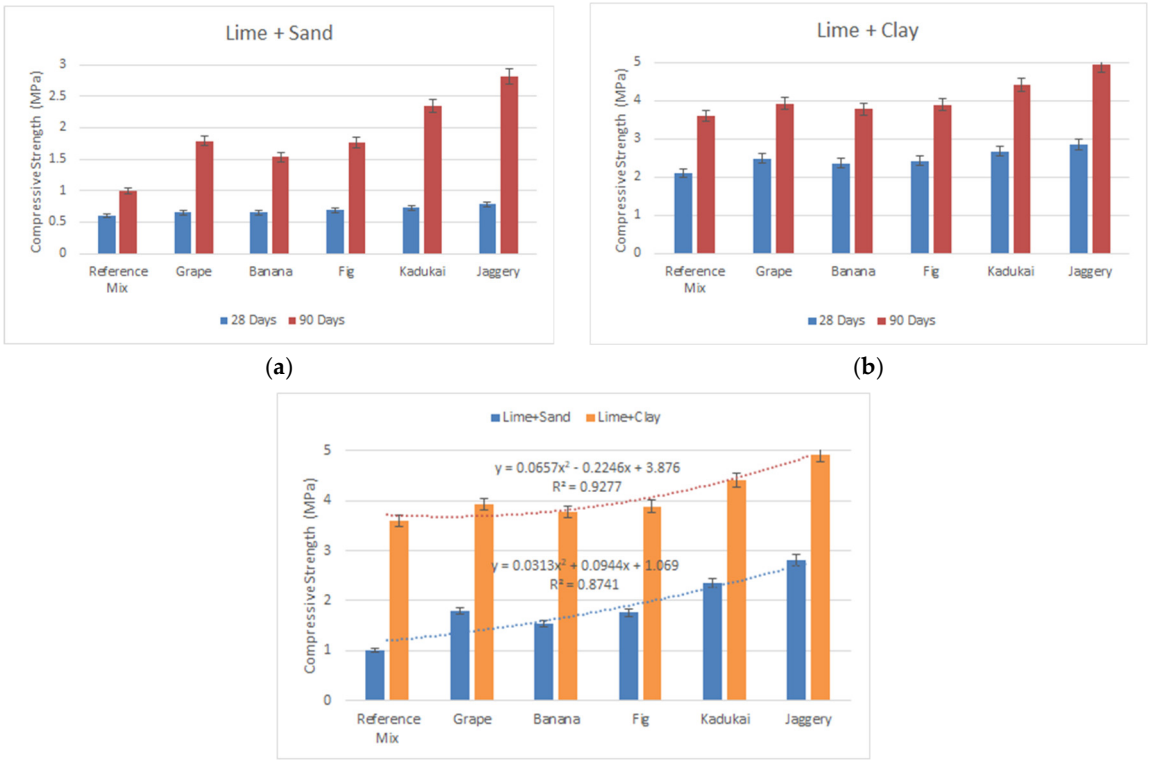

Figure 7. Compressive strength: (**a**) 28 and 90 curing days for lime–sand mixtures, (**b**) 28 and 90 curing days for lime–clay mixtures, (**c**) comparison between lime–sand and lime–clay mixtures at 90

curing days. Error bars indicate standard deviation. A multiple regression model was formulated using the compressive strength values; R2 values of 0.927 for lime–clay and 0.874 for lime–sand mixes were obtained, which established an excellent accuracy of the experimental values [56].

4.1.2. Porosity and Density

Porosity and density are crucial factors on which the compressive strength is directly dependent. Porosity and density imprint the water permeability, which further affects the thermal and electrical conductivity of the mortars. The higher the porosity, the lesser will be the strength; in fact, an increase in pore space results in a poor distribution of forces under compression and the early failure of samples. On the other hand, the higher the density, the higher is the expected strength, i.e., the samples will perform better in compression as the interstitial spaces are reduced.

Table 4 lists the porosity and density parameters for the studied samples, indicating higher porosity values in reference mixes than in organic limes; these porosity values would justify the lower compressive strength of the reference mixtures in respect to the organic ones.

Table 4. Porosity and density for test samples.

		Reference Mix	Grape	Banana	Fig	Kadukai	Jaggery
Porosity	Lime + Sand	26	15	15.3	16.4	18	19
	Lime + Clay	22	11	13	14	15	16
Density	Lime + Sand	1.8	2.1	1.92	2	2.3	2.4
	Lime + Clay	2.5	3.1	2.9	2.9	2.6	2.8

The addition of organics was found to reduce the porosity, which can be interpreted as a result of the enhanced reaction of lime and organics turning in the formation of smaller pores. A slight reduction of porosity was also observed in the lime–clay reference mix in respect to the lime–sand mix; this result might be explained by hydrated phase precipitation in the pore spaces.

Density was also found to increase with the addition of organics up to 25%, according to the calculated porosity values and compressive strength.

4.1.3. Thermal Conductivity

The thermal conductivity of a mortar mix is dependent on several factors, namely porosity, density, moisture content, volume of material, type and degree of saturation, nature and amount of aggregates, etc. [34,54,55,57–59]. The void ratio, or packing density, greatly affects the thermal conductivity of limes [54,58]; an increase in porosity, and thus air voids, implies a reduction in weight, density, and thermal performance when compared to a material with less air content having the same volume. Moreover, the composition of the lime paste, the hydration degree, and the calcium-silicate-hydrated fraction imprint the final properties of the mixture [54].

In the modified mixtures, the addition of organics reduced the thermal conductivity parameters for both lime–sand and lime–clay mixtures (Figure 8). In the grape, banana, and jaggery mixtures, lime–clay samples showed higher thermal conductivity than the lime–sand counterparts, except for fig and kadukai, for which the lime–sand mixtures showed higher thermal conductivity values than other mixes.

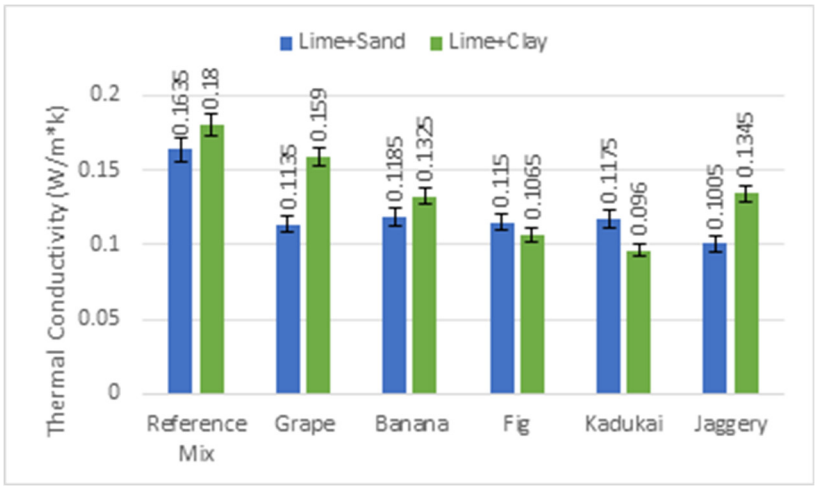

Figure 8. Thermal conductivity for reference and organic lime mortars; comparison between lime–sand (blue) and lime–clay (green) mixes.

In the case of lime–sand mixes, organic additives reduced the thermal conductivity; in fact, it was about 25% less than in the reference mixture. Usually, an increase in air voids determines a reduction of density and thermal conductivity. However, in these mixtures, the addition of organics determined a reduction of porosity and an increase in density and mechanical strength. Thus, merely the density and the porosity cannot be enough to explain the mortar behavior; in fact, other relevant parameters are moisture content and pore-size distribution [59–61]. Overall, thermal conductivity seems to decrease with increasing hydration degree; in organic mixtures the presence of polysaccharides from organics acts as moisture-retained agents determining an increase in hydration degree [62]. Moreover, in these modified mixtures the boost of CO_2 supplied by the fermentation of organics and presence of alcoholic components determines the transformation of calcium hydroxide into calcium alkoxide and calcium carbonate, with the precipitation of different polymorphs like metastable vaterite and aragonite rather than stable calcite [63]. This peculiar lime composition might be considered responsible for the reduction in thermal conductivity observed in the organic mixtures.

The reduction trend could also be observed in lime–clay mixtures; in fact, the organic mixtures exhibited lower thermal conductivity than the reference sample. In the grape, banana, and jaggery lime–clay mixtures the thermal conductivity homogeneously increased with respect to the lime–sand counterparts. This behavior could be related to the occurrence of Calcium-Aluminum-Silicate-Hydrate (CASH) phases formed in the hydraulic mixture. The thermal conductivity of these phases is higher than lime (0.13–0.15 W/m-k for lime and 0.9–3.5 W/m-k for hydrated phases) [57]. In lime–clay mixtures, the silicate and aluminate ions interact with Ca^{2+} and determine the formation of CASH gel, exhibiting higher thermal conductivity properties. During these reactions, the hydrated phases occupy space initially occupied by water. This implies a reduction of porosity, as the spaces are now filled by CASH gel, and thus a higher density in the mortar paste, according to values reported in Table 4. These reactions are competitive with portlandite to calcite formation and their extent depends on the cement/water ratio, the CO_2 content in the air, the relative humidity, and the porosity [61]. Previous studies carried out by the authors demonstrated that in lime mortars the carbonation is only imprinted by the absorption of free carbon-dioxide from the atmosphere. Thus the exterior part of lime mortars is carbonated while the inner part of mortars remains un-carbonated; otherwise when organics are added into the mixture the organic fermentation boosts the availability of carbon-dioxide in the whole mix volume, thus favoring the precipitation of more calcite [21,63,64].

It is understandable that in organic lime–clay mixtures the competition between the two reactions is credibly shifted toward calcite formation, with consequently relative lower thermal conductivity values in respect to the reference mixture. At the same time, the composition of the

cement paste and the higher moisture retention due to the organics contribute to the overall reduction of thermal conductivity. The description of these reactions would need further investigations to better understand how the nature of organics imprints the extent and the rate of competition between calcite and hydrated phases reactions.

Summarizing, the addition of organics seems to improve the structures' thermal efficiency. A low thermal conductivity resulted in a higher thermal resistance than reference mortars, thereby improving the insulation properties of the building structures.

4.1.4. Electrical Conductivity

Electrical conductivity is usually a function of aggregate volume fraction, saturation, density, and pore size distribution [65,66]. The interconnection of material particles and interconnection among pores tend also to affect the electrical conductivity [67,68]. Moreover, the salinity of water used for mixing lime paste greatly influences the electrical conductivity. Generally, high water–cement ratios determine higher electrical conductivity due to an increasing of dissolved ions. The electrical conductivity values measured in the studied samples are summarized in Figure 9.

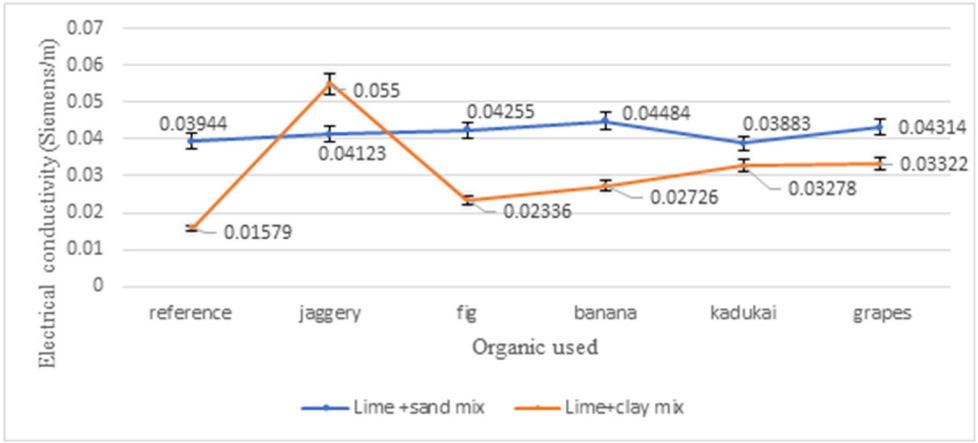

Figure 9. Electrical conductance for lime–sand and lime–clay mixtures.

Lime–sand mortars exhibited higher electrical conductivity respect to lime–clay mortars. Besides, the mixes with organics exhibited higher electrical conductivity compared to the reference mix. This behavior might be explained by the modified chemical composition of the paste imprinted by the organics, which increases the pH and enhances the movement of the electrons.

Thus far, the net differences between sand–limes and clay–limes can be explained based on the extent of reactions occurring in the mortar paste. In clay–limes, the faster consumption of free ions for the formation of hydrated phases gel can be considered responsible for the reduction in electrical conductivity [69]. Clay–lime mixed with jaggery deviated from the general trend, suggesting the extent of interactions leading to a relevant change in pore structure and pore interconnection, which would in turn need further studies and analysis.

4.2. Lime Mortars from Heritage Monuments

As a comparison, Table 5 shows the electrical conductivity and composition of specimens taken from various heritage sites in India. The electrical conductivity in samples from heritage monuments was found to have higher values with respect to the reverse-engineered samples, credibly because of degradation processes that modify the chemical composition of historical samples. Moisture circulation and soluble salts represent the main degradation agents responsible for such modifications; moreover, the use of modern incompatible materials and wrong conservation practices contribute to the degradation of building materials. The samples were found to have a higher pH value, which favors the movement of electrons through the material, thus affecting its electrical conductivity. Acid rains and other weathering processes were also responsible for the

change in the pH. Nevertheless, the electrical conductivity in specimens from the heritage structures showed high resistivity or low electrical conductivity as compared to the tested controlled samples without organics and the conventional cement concrete, with a value of about 0.988 S/m [65,70,71]. The tested mortar samples, which were made to resemble to the ancient mortars as closely as possible, were found to have very low electrical conductivity in respect to conventional concretes, attesting the advanced engineering and quality of ancient mortars.

Table 5. Electrical conductivity for specimens from heritage sites in India.

Sample No.	Sample Details	Organic Constituents	Conductivity (Siemens/m)	pH Value
1.	Thiruvananthapuram temple	Kadukai, Cactus, Jute fibers, Sweet potato	0.1407	3.49
2.	Charminar	Kadukai, Jaggery, Egg white	0.1294	3.36
3.	Vadakatham Temple	Kadukai, Jaggery, Sweet potato	0.2769	3.42
4.	Thiruvananthapuram Temple	Cactus, Neelamari, Kadukai, Sweet Potato, Lotus Leaves, Hibiscus Leaf, Jute fibers, Cow dung, Gum arabica, Curd	0.2323	4.1
5.	Naganathaswamy Temple	Kadukai, Jaggery	0.3105	3.78
6.	Sacred Groves Auroville	Kadukai, Jaggery	0.2149	3.4
7.	Thanjavur Palace	Kadukai, Jaggery	0.4205	4.66
8.	Sacred Groves Auroville	Kadukai, Jaggery	0.4436	4.55

In the frame of the present investigation, it is very pertinent to note that the relationship between electrical conductivity and skin depth is inversely related i.e., skin depth decreases with higher conductivity. Hence, the appropriate choice of the mortar mix is essential to evaluate the optimum electrical conductivity values for a building structure, especially when it is necessary to meet requirements in lightning strike protection.

5. Simulation of the Role of Electrical Conductivity and Skin Effect in Heritage Structures Due to Lightning Strikes

5.1. Modeling and Analysis of Skin Depth in Heritage Monuments

In order to evaluate the role played by organics in electrical conductivity and skin effect, we performed electromagnetic field simulation studies and modeling by using electrical conductivity values measured on reverse-engineered organic mortars and mortar samples of heritage structures. In respect to heritage structures, samples obtained from the Charminar monument were used for the simulation; in fact, the monument is mainly built in organic lime mortars. Furthermore, it is important to note that the Charminar was struck by several lightning strikes on its south-western minaret [11] in the past. From the context of laboratory samples, kadukai and jaggery mixes were used.

Electromagnetic field modeling and simulation analysis for assessing the skin depth were developed based on a 2-D representation of the structure as it was found appropriate considering the inherent geometrical symmetry of Charminar monument; the layout of the monument is depicted in Figure 10 a–c, which clearly substantiates this aspect.

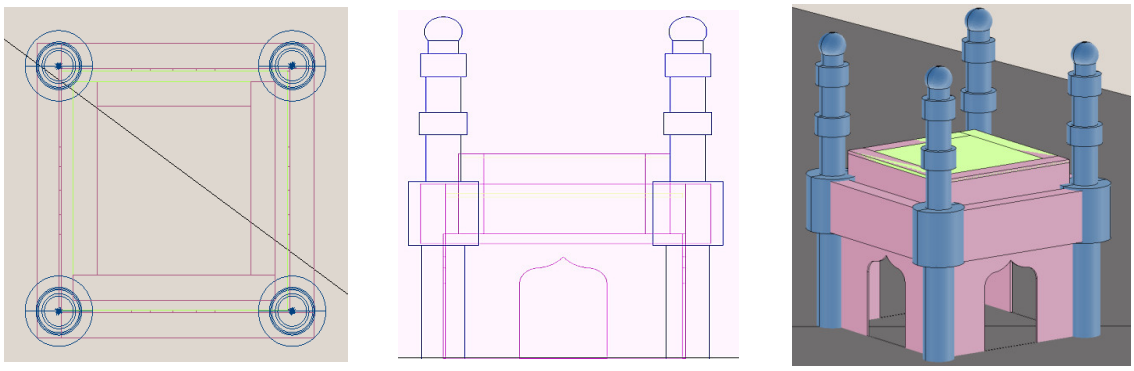

(**a**) (**b**) (**c**)

Figure 10. (**a**) Plan View of Charminar; (**b**) Elevation View; (**c**) 3D layout of mosque.

Computed values of the skin depth for the various lime mortars at different frequencies are presented in Figure 11. The obtained results suggested that at a frequency of 10 kHz, skin depth is higher than those for frequencies at 250 and 800 kHz; all the samples of skin depth displayed the same trend. Lime mortar from heritage monuments showed the maximum value of conductivity but minimum skin depth penetration at various frequencies.

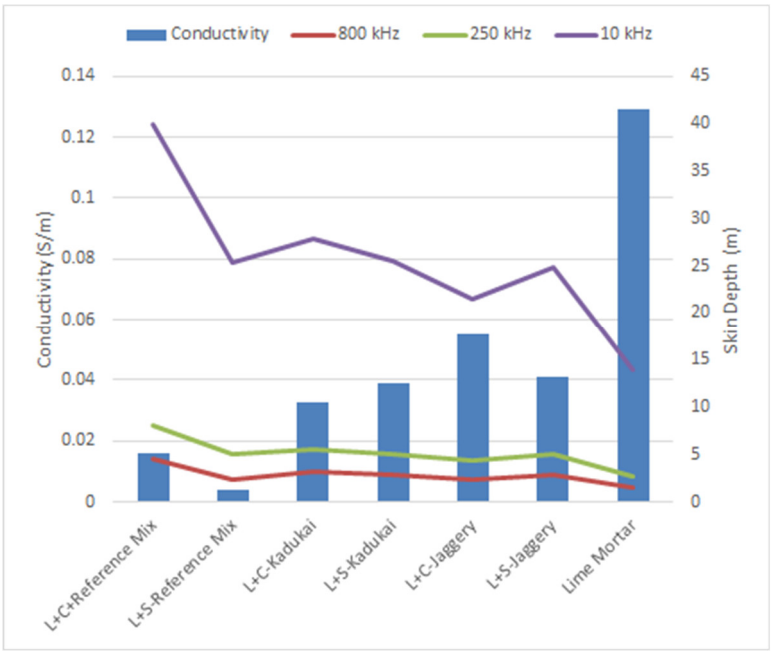

Figure 11. Values of electrical conductivity and computed skin depth for varying frequencies simulated during a lightning strike. L+C: lime + clay; L+S: lime + sand.

During simulation, the Charminar monument was also taken up for modeling. The first step involved generating the 2-dimensional layout drawing of the monument and modeling it using the PDE toolbox with the scale of X–Y ordinates fixed in meters. Secondly, the boundary conditions (Dirichlet and Neumann) were specified. Finally, appropriate values of electrical characteristics relevant to lightning were specified to enable obtaining solutions for partial differential equations using FEM. Such parameters and characteristics were taken up for detailed comparison and analysis to ascertain the role of skin depth due to varying frequencies and based on variations in material properties.

Figure 12 depicts the layout of the Charminar monument modeled using the PDE Toolbox, while Figure 13 a,b depicts the formulation of boundary conditions and electrical parameters for a FEM-based solution, which governs the formulated partial differential equations.

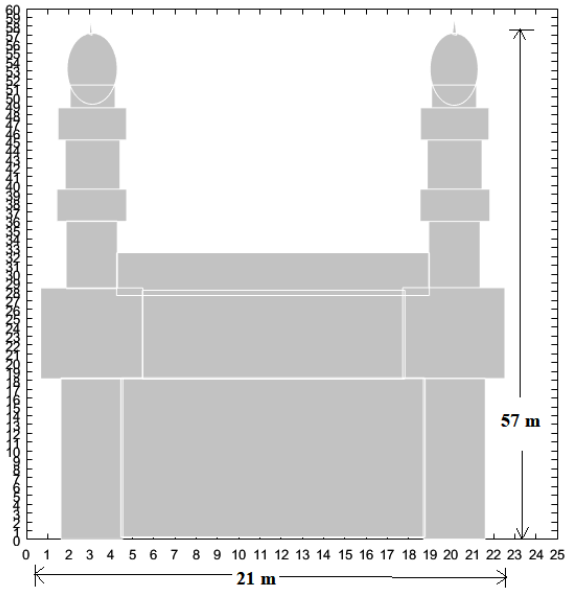

Figure 12. Modeled layout of drawing of Charminar using the Partial Differential Equation (PDE) toolbox for skin depth analysis.

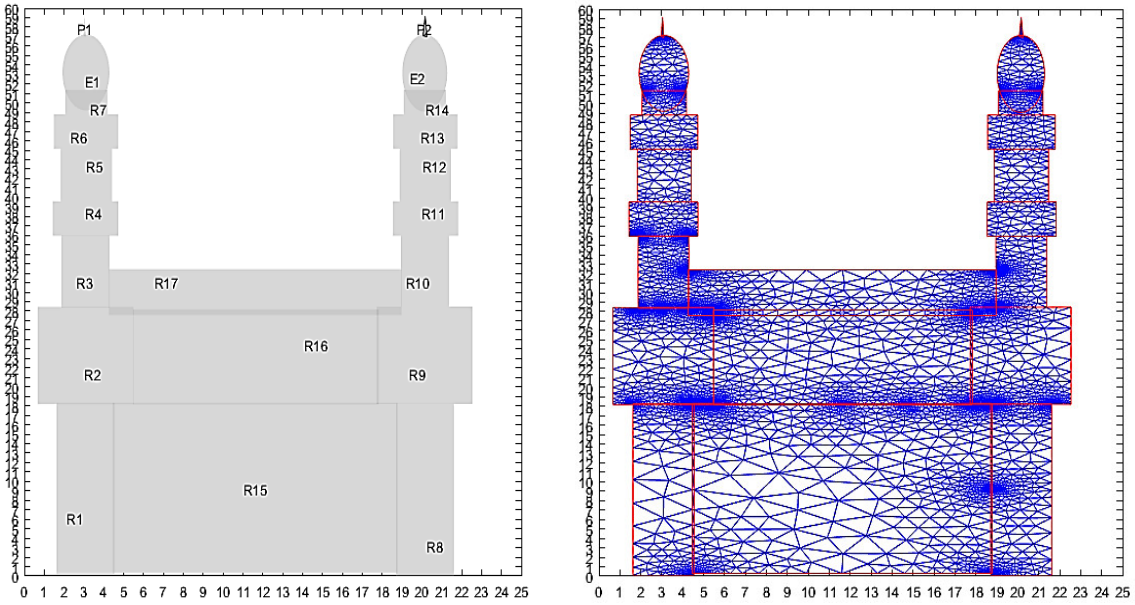

(**a**) (**b**)

Figure 13. (**a**) Layout of the Charminar Monument for simulation of the role of electrical conductivity and skin depth; (**b**) simulation of Finite Element Method (FEM)-based solution of the heritage structure.

Since the skin depth is directly related to the electrical resistivity (i.e., electrical conductivity) and to the frequency, simulation studies were considered for various ranges of electrical conductivity for the same mortar mix. A case study depicted in Figures 14 and 15 represents a plot of the depth of penetration for the reference mix (lime–clay) for electrical conductivity (σ) of 0.01579 S/m at frequencies of 250 kHz (in line with stipulations laid out in IEC 62305 [25]) and 10 kHz (as per CIGRE WG 33.01 [29]). The depth of penetration is lesser for 250 kHz as compared to 10 kHz since the extent of the intensity of the electric field is more on the outer periphery of the structure than the inner location of the monument. The transition in the electric field intensity based on color variations from red (maximum intensity) to blue (minimum intensity) makes this aspect evident. In the case of higher frequencies, the transition from red to green is more graded, whereby there is a transition

from red to green and finally to blue. Hence, the extent of damage due to lightning strikes with a higher range of frequency is much lesser than those related to repeated strikes whose frequencies are of the order of 10 to 50 kHz. This aspect is a very significant deduction during the analysis.

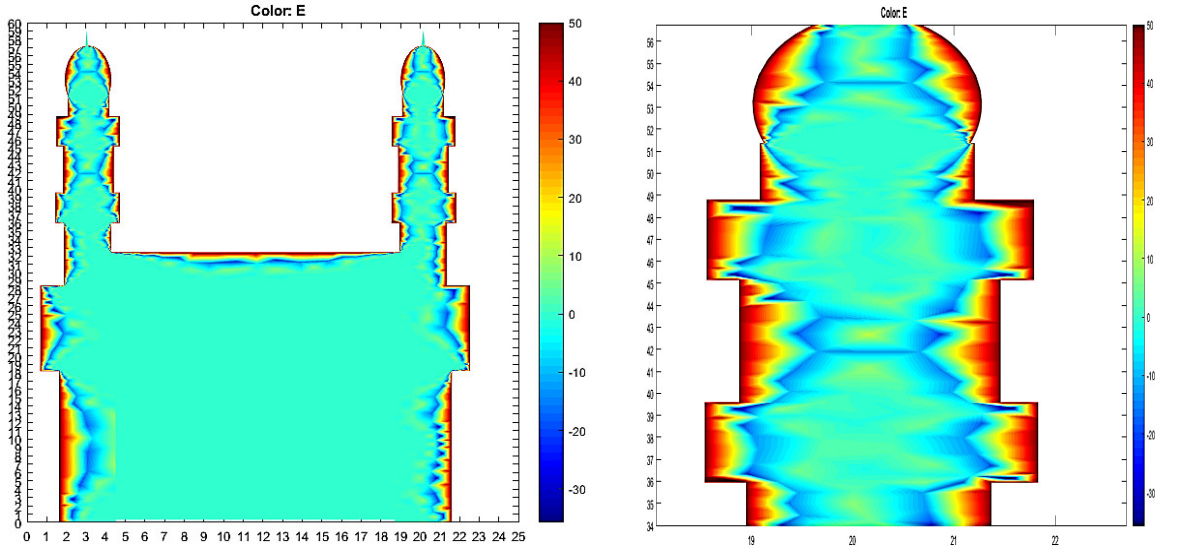

(**a**) (**b**)

Figure 14. (**a**) Plot of simulation for obtaining skin depth with σ = 0.02 at a frequency of 250 kHz; (**b**) detailed view of skin depth and depth of penetration at vulnerable points of the structure.

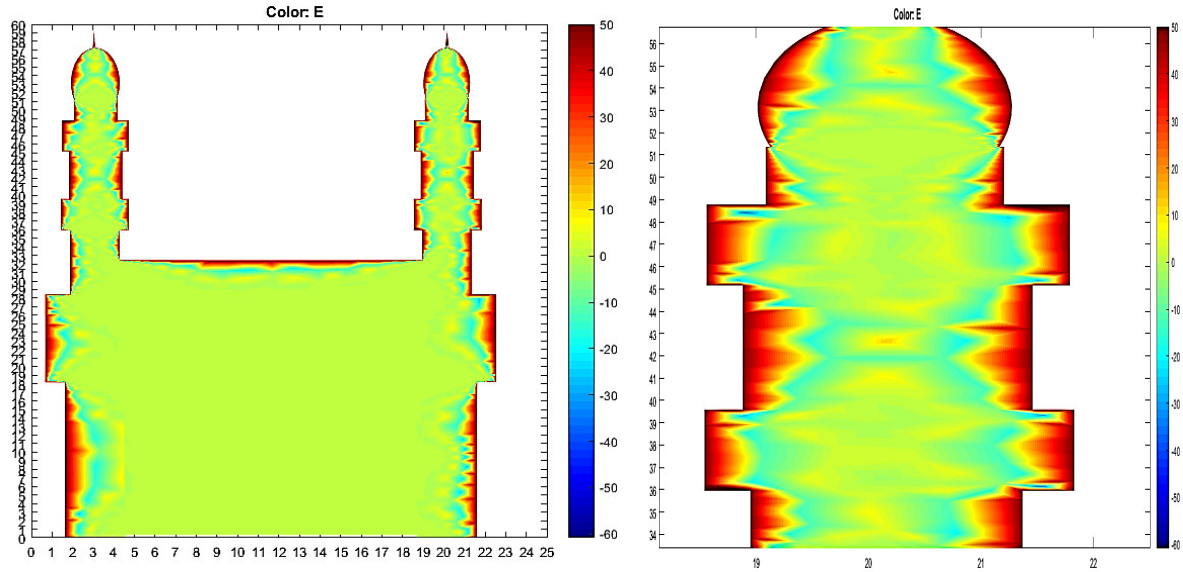

(**a**) (**b**)

Figure 15. (**a**) Plot of simulation for obtaining skin depth with σ = 0.02 at a frequency of 10 kHz; (**b**) detailed view of skin depth and depth of penetration at vulnerable points of the structure.

For the purpose of comparison and detailed analysis, simulations were carried out by considering different mixes at the same frequency. Conductivity values measured for the reference laboratory mix (lime–clay), heritage structure mortar from Charminar, and one of the best performing organic mixtures (kadukai in lime–clay mix) were considered. In addition, a simulation was carried out considering electrical conductivity in conventional cement concrete (0.998 S/m; [66,71]). It is worth mentioning that during the simulation studies the electrical parameters, such as dielectric constant (ε), magnetic permeability (μ), and the material composition of the lime mortar, were considered

homogeneous; in real-time these values may have statistical variations due to effects of temperature, moisture, humidity, etc. Additionally, since cement and lime invariably in their basic form are non-magnetic [72], the magnetic permeability was assumed to be unitary during the simulation studies and analysis.

Figure 16 demonstrates the results of the simulation studies and analysis at the same frequency (10 kHz), which were carried out on four binding materials, namely the reference mix, a sample from the heritage monument, a sample based on lime–clay + kadukai, and a sample of cement concrete mix.

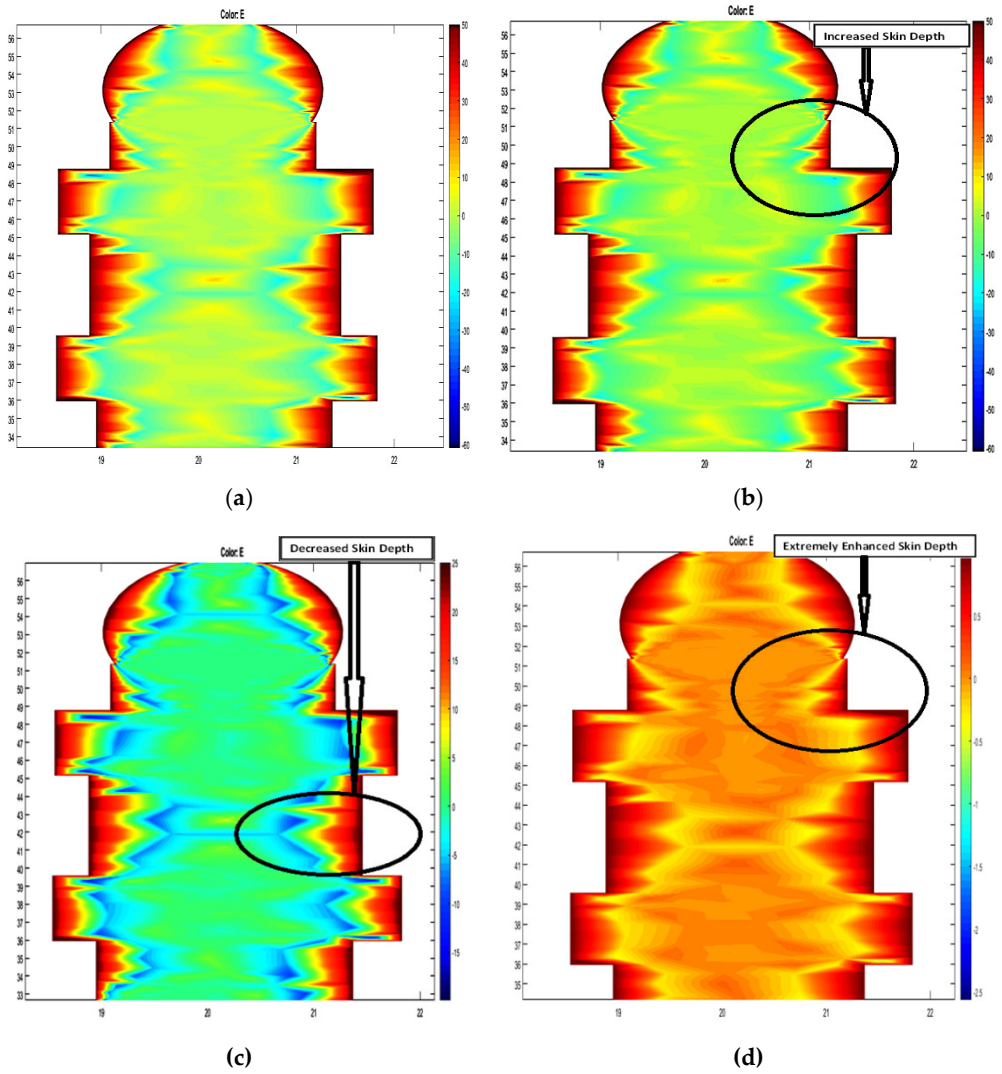

Figure 16. Comparison for depth of penetration at 10 kHz for varying lime mortar mixes: (**a**) reference mix (lime–clay), (**b**) lime mortar of the heritage monument (from Charminar), (**c**) lime-clay + kadukai, and (**d**) cement concrete mix. In (a–c) dielectric permittivity (εr) = 7 and magnetic permeability (μr) = 1–3; in (d) dielectric permittivity (εr) = 12–29 and magnetic permeability (μr) = 1.

The results of the simulation for different mixes evidenced that organic mixtures (lime–clay + kadukai) displayed a decrease in the depth of penetration (skin depth), indicating their ability in ensuring better response to lightning strikes. This aspect is evident from the simulation result shown in Figure 16c, which indicates that the electric field gets graded from maximum (denoted by red color) to the less intense field (indicated in green) and gradually to the minimum (shown in blue).

The proposed simulation thus demonstrated the importance of traditional organic mixtures in reducing the extent of the skin depth in heritage monuments.

5.2. Validation of Skin Depth Simulation during Lightning Strikes

The validation of models simulating the impact of lightning strikes on monuments is a challenging task. The International Electrotechnical Commission (IEC) standards supply fundamental guidelines for the interpretation of structural damages due to lighting strikes [25,27] and fundaments for the interpretation and validation of damage models.

In respect to the Charminar monument, in 2019 a lightning strike caused the collapse of the south-west minaret, necessitating its restoration [11]. The damages' photo documentation of the monument after the event (Figure 17) evidences crumbling and cracks on the stucco ornaments of the minaret [11], whose areas exactly correspond to vulnerable points evidenced by the simulation reported in Figure 16b, thus cross-validating the proposed model.

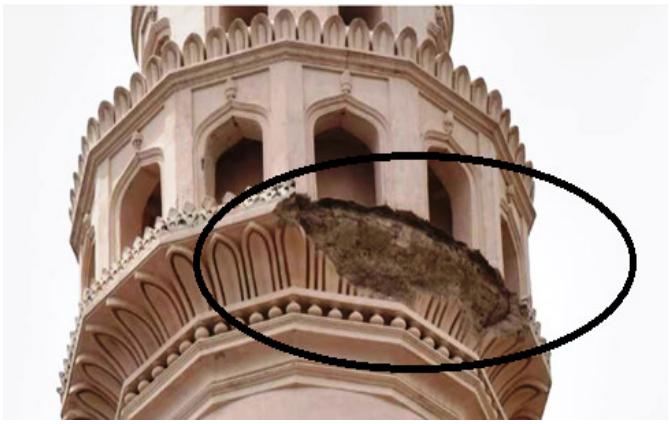

Figure 17. Damaged ornamentation stucco of the south-west minaret in Charminar Mosque.

6. Conclusions

The most relevant findings of this investigation are summarized as follows:

1. The laboratory testing on reverse-engineered mixes demonstrated that the electrical conductivity in organic mortars is less than conventional concrete materials and slightly higher than reference mixes; nevertheless, organic mortars exhibited higher strength and ensured good thermal insulation, improving the building thermal efficiency.
2. Lime-clay + jaggery mixes demonstrated superior properties in ensuring considerably lower skin depth and good thermal conductivity characteristics. Similarly, lime–sand + kadukai mixes have showed characteristics ensuring low skin depth values and less conductivity values as compared to traditional lime mortars used in heritage structures. These mixtures are expected to result in lesser damage to building structures.
3. The numerical simulations carried out on laboratory and heritage samples demonstrated the reliability of traditional mortars that are characterized by a mixture of organics, which in turn aids in improving the building's resilience to lightning strikes. It is important to note that the calculated skin depth was in fact lower than for cement mortars.
4. The electrical conductivity values obtained on heritage samples were in considerable agreement with a few other studies on traditional heritage mortars, which in turn strengthens the results of the analysis.
5. The selection of additives in manufacturing repair mortars needs careful analysis of their impact on the thermal and electrical conductivity of the final mix.
6. Traditional green ingredients and knowledge from the past might provide insights in the design of environmentally sustainable materials in building construction; the organic mixes seem to assure improved thermal efficiency and resilience to natural hazards.
7. The organic mixtures may provide a valuable alternative in manufacturing repair mortars, ensuring useful thermal conductivity characteristics (i.e., thermal insulation) and electrical conductivity properties, which in turn may lead to lesser skin depth than cement and concrete.

8. A comprehensive analysis based on thermal and electrical conductivity testing becomes extremely important to ensure appropriate lightning strike protection of building structures.
9. Possible avenues for further research would comprise the development of new mortar mixes by using aggregates and additives guaranteeing low resistivity (in the order of a few tens of Ω-m) to obtain better protection, shielding and grounding against lightning strikes.

Author Contributions: Conceptualization, T.S. and V.S.; Methodology, T.S. and V.S.; Software, T.S., V.S. and M.F.; Validation, T.S. and M.F.; Formal analysis, V.S., S.R. and K.K.; Investigation, T.S., V.S. and S.J.; Resources, T.S. and V.S.; Data curation, S.R. and S.J.; Writing-Original Draft Preparation, T.S. and V.S.; Writing-Review & Editing S.R. and M.F.; Visualization, S.R. and K.K.; Supervision, T.S., V.S. and M.F.; Project administration, T.S. and V.S.; Funding acquisition, T.S., V.S. and M.F. All authors have read and agreed to the published version of the manuscript.

Funding: This research was funded by Department of Science and Technology (DST), Government of India and Ministry of Science, Technology and Research (MSTR), Sri Lanka, under the India-Sri Lanka Bilateral Research Project, Grant Number DST/INT/SL/P-14/2016/C&G. The APC was funded by India-Sri Lanka Bilateral Research Project, Grant Number DST/INT/SL/P-14/2016/C&G.

Acknowledgments: The authors would like to acknowledge the support of Indian Institute of Technology (IIT), Madras for allowing the use of the Resipod© and Compression Testing Equipment facility. The authors are also extremely grateful to the Archaeological Survey of India (ASI), New Delhi, for according permission, approval and for their continued support to undertake lightning protection studies.

Conflicts of Interest: The authors declare no conflict of interest.

References

1. Aslam, Z.; Ardemagni, M. Introducing Young People to the Protection of Heritage Sites and Historic Cities UNESCO ATHAR Programme (Conservation of Archaeological Heritage in the Arab Region), ICCROM & UNESCO, 2006. Available online: https://www.iccrom.org/sites/default/files/ICCROM_09_ManualSchoolTeachers_en.pdf (accessed on 23 May 2020).
2. Pedersoli, J.L. A guide to Risk Management of Cultural Heritage, Canadian Conservation Institute, ICCROM, Italy, 2016. Available online: https://www.iccrom.org/wp-content/uploads/Guide-to-Risk-Managment_English.pdf (accessed on 23 May 2020).
3. Cristi, J. NICO, Natural Hazards—A threat to immovable cultural heritage. A review. *Int. J. Cons. Sci.* **2017**, *8*, 375–388.
4. Illiyas, F.; Mohan, K.M.; Pradeep Kumar, S.K.M. Lightning Risk in India challenges in disaster compensation. *Econ. Political Wkly.* **2014**, *23*, 23–27.
5. Sreedhar, S.; Srinivasan, V. Lightning strokes and its effect on historical monuments, heritage properties and important landmarks a detail perspective of traditional and scientific methods of lightning protection system. *Int. J. Eng. Tech.* **2018**, *7*, 784–794.
6. Kalasam on Big Temples's 'Rajarajan Thiruvayil' Damages in Lightning Strike. Available online: https://www.thehindu.com/news/national/tamil-nadu/Kalasam-on-Big-Temples-lsquoRajarajan-Thiruvayil-damaged-in-lightningstrike/article15719847.ece (accessed on 23 May 2020).
7. Temple Bears Lightning Brunt. Available online: https://www.telegraphindia.com/states/odisha/temple-bears-lightning-brunt/cid/1507044 (accessed on 23 May 2020).
8. Part of 500-Year-Old Ratneshwar Mahadev Temple Collapses due to Lightning. Available online: https://www.dnaindia.com/india/report-varanasi-part-of-500-year-old-ratneshwar-mahadev-temple-collapses-due-to-lightning-2188737 (accessed on 23 May 2020).
9. Centuries-Old Temple Damaged in Lightning Strike. Available online: https://www.orissapost.com/centuries-old-temple-damaged-in-lightning-strike/ (accessed on 23 May 2020).
10. Lightning Strikes Heritage Site in Khajuraho, Damages Temple. Available online: https://www.hindustantimes.com/bhopal/lightning-strikes-heritage-site-in-khajuraho-damages-temple/story-cL4o6IwUsltvSRcytL20KM.html (accessed on 23 May 2020).

11. Southwest Minaret had Collapsed Due to Lightning. Available online: https://timesofindia.indiatimes.com/city/hyderabad/southwest-minaret-had-collapsed-due-to-lightning/articleshow/69159868.cms?utmsource=contentofinterest&ut+medium=text&utm+campaign=cppst (accessed on 23 May 2020).
12. Old Goa Structures Now Lightning proof. Available online: https://timesofindia.indiatimes.com/city/goa/5-old-goa-structures-now-lightning-proof/articleshow/68193855.cms (accessed on 23 May 2020).
13. Patel, K. Effects of Lightning on Building and Its Protection Measures. *IJEAT*, **2013**, *2*, 182–185.
14. Hummel, R.E. *Understanding Materials Science History, Properties, Applications*, 2nd ed.; Springer: New York, NY, USA, 2005.
15. Ipekoglu, B.; Boke, H.; Cizer, O. Assessment of material use in relation to climate in historic buildings. *Build Env.* **2007**, *42*, 970–978.
16. Thirumalini, S.; Ramadoss, R.; Sekar, S.K.; Nambirajan, M. Knowing from past- Ingredients and technology of ancient mortar used in Vadakumnatham temple. *J. Build. Eng.* **2015**, *4*, 101–112.
17. Holland, N.L.; Nichols, A.; Nichols, J. The Use of Hydrated Lime in Concrete as a Cement Replacement: Effect on Compressive Strength. In *Lime: Building on the 100-Year Legacy of the ASTM Committee C07*; Thomson, M., Brisch, J., Eds.; ASTM International: West Conshohocken, PA, USA, 2012; pp. 106–112.
18. Singh, V.K.; Mandal, U.K. Effect of Lime on the Properties of Portland Cement. *Trans. Indian Ceram. Soc.* **1980**, *39*, 161–164.
19. Abdel-Mooty, M.; Khedr, S.; Mahfouz, T. Evaluation of lime mortars for the repairs of historic building. In: *Structural Studies, Repairs and Maintenance of Heritage Architecture XI*; Brebbia, C.A., Ed.; WIT Press: Wessex UK, 2009; pp. 209–220.
20. Ramadoss, R.; Ahamed, A.; Thirumalini, S. Alternative Approach for Traditional Slaking and Grinding of Air Lime Mortar for Restoration of Heritage Structures: Natural Polymer. *J. Archit. Eng.* **2019**, *25*, 04019017.
21. Jayasingh, S.; Thirumalini, S. Influence of organic additive on carbonation of air lime mortar—Changes in mechanical and mineralogical characteristics. *Eur. J. Environ. Civ. Eng.* **2020**, doi:10.1080/19648189.2020.1731716.
22. Nag, A.; Rakov, V.A. Positive lightning: An overview, new observations, and inferences. *J. Geophys. Res. Atmos.* **2012**, *117*, D08109.
23. Saslow, M.W. Capacitance. In *Electricity, Magnetism, and Light*; Saslow, M.W., Ed.; Academic Press: Cambridge, Massachusetts USA, 2002; pp. 227–280.
24. Pasek, M.A.; Hurst, M. A Fossilized Energy Distribution of Lightning. *Sci. Rep. Nat.* **2016**, *6*, 30586.
25. *IEC 62305-3:2010, Protection Against Lightning—Part 3: Physical Damage to Structures and Life Hazard*, 2nd ed.; International Electrotechnical Commission: Geneva, Switzerland, 2010.
26. Borovsky, J.E. An electrodynamic description of lightning return strokes and dart leaders. *J. Geophys. Res.* **1995**, *100*, 2697–2726.
27. *IEC 62305-1:2010, Protection Against Lightning- Part 1: General Principles*, 2nd ed.; International Electrotechnical Commission: Geneva, Switzerland, 2010.
28. Anderson, R.B.; Eriksson, A.J. Lightning Parameters for Engineering Applications. *Electra* **1980**, *69*, 65–102.
29. Rakov, V.A. Lightning parameters for engineering applications—An update on CIGRE WG C4.407 activities. In *International Symposium on Lightning Protection (XI SIPDA)*; IEEE: Fortaleza, Brazil, 2011; pp. 294–297, doi:10.1109/SIPDA.2011.6088434.
30. Gomes, C.; Ab Kadir, M.Z.A.; Izadi, M.; Gomes, A. Lightning current and voltage distribution of large axially symmetric buddhist stupa in Sri Lanka. In Proceedings of the *2014 International Conference on Lightning Protection (ICLP), Shanghai, China,* 11–18 October 2014; IEEE: Shanghai, China, 2014; pp. 1637–1651, doi:10.1109/ICLP.2014.6973392.
31. Katunin, A.; Krukiewicz, K. Preliminary Analysis of Thermal Response of Dielectric and Conducting Composite Structures during Lightning Strikes. *Comp. Theory Pract.* **2016**, *16*, 8–14.
32. Elmi, C.; Chen, J.; Goldby, D.; Giere, R. Mineralogical and compositional features of rock fulgurites: A record of lightning effects on granite. *Am. Mineral.* **2017**, *102*, 1470–1481.
33. Millen, S.L.J.; Murphy, A.; Catalanotti, G.; Abdelal, G. Coupled Thermal-Mechanical Progressive Damage Model with Strain and Heating Rate Effects for Lightning Strike Damage Assessment. *Appl. Compo. Mater.* **2019**, *26*, 1437–1459.

34. Stefanidou, M.; Assael, M.; Antoniadis, K.; Matziaroglou, G. Thermal Conductivity of Building Materials Employed in the Preservation of Traditional Structures. *Int. J. Thermophys.* **2010**, *31*, 844–851.
35. Lime Mortars in Traditional Buildings, Historic Environment Scotland Historic Scotland. Available online: https://www.historicenvironment.scot/archives-and-research/publications/publication/?publicationId=85ced9f0-474d-4ec6-8dd6-a59100fc306f (accessed on 23 May 2020).
36. Ashurst, J. *Conservation of Ruins*, 1st ed.; Butterworth-Heinemann: Oxford, UK, 2007.
37. Uygunoğlu, T.; Bekir Topçu, İ.; Çınar, E.; Resuloğulları, D. Electrical and mechanical properties of historical mortars in Bursa/Turkey. *Revista de la Construcción, SciELO Anal.* **2019**, *18*, 54–67.
38. Ravi, R.; Thirumalini, S.; Taher, N. Analysis of ancient lime plasters—Reason behind longevity of the Monument Charminar, India a study. *J. Build. Eng.* **2018**, *20*, 30–41.
39. Thirumalini, S.; Ramadoss, R.; Sekar, S.K. Revealing the ancient secret of lime mortar exposed to marine environment used in and around Padaleeswarar temple, Tamil Nadu, India. In *Proceedings of the 4th Historic Mortars Conference—HMC 2016*; Papayianni, I., Stefanidou, M., Pachta, V., Eds.; Aristotle University of Thessaloniki: Thessaloniki, Greece, 2016; pp. 93–103.
40. Thirumalini, S.; Ramodass, R. Analysis and characterization of third century ancient mortars at Subramanyaswamy Temple rediscovered after the 2004 tsunami near Mamallapuram shore, India. *Int. J. Conserv. Sci.* **2018**, *9*, 25–38.
41. Thirumalini, S.; Sekar, S. Heritage Lime Mortar Characterization and Simulation. Ph.D. Thesis, School of Mechanical and Building Sciences, Vellore Institute of Technology, Vellore, India, 2014.
42. Rodriguez-Navarro, C.; Vettori, I.; Ruiz-Agudo, E. Kinetics and mechanism of calcium hydroxide conversion into calcium alkoxides: Implications in heritage conservation using nanolimes. *Am. Chem. Soc.* **2016**, *32*, 5183–5194.
43. Fang, S.Q.; Zhang, H.; Zhang, B.J.; Zheng, Y. The identification of organic additives in traditional lime mortar. *J. Cult. Herit.* **2014**, *15*, 144–150.
44. Thirumalini, S.; Ramadoss, R.; Rajesh, M. Experimental investigation on physical and mechanical properties of lime mortar: Effect of organic addition. *J. Cult. Herit.* **2018**, *31*, 97–104.
45. *IS 6932:1973, Part I, Methods of Tests for Building Limes*; Bureau of Indian Standards: New Delhi, India, 1973.
46. *IS 6932:1973, Part V, Methods of Tests for Building Limes, Determination of Hydrated Oxide*; Bureau of Indian Standards: New Delhi, India, 1973.
47. *IS 712: 1984, Specification for Building Limes*; Bureau of Indian Standards, New Delhi, India, 1984.
48. *IS 6932: 1973, Part VIII, Methods of Tests for Building Limes-Determination of Workability*; Bureau of Indian Standards, New Delhi, India, 1973.
49. *IS 2386: 1963, Part I, Methods of Test for Aggregates for Concrete*; Bureau of Indian Standards, New Delhi, India, 1963.
50. *IS 6932: 1973, Part VII, Methods of tests for building limes- Determination of Compressive and Transverse Strengths*; Bureau of Indian Standards, New Delhi, India, 1973.
51. *IS 516: 1959, Method of Tests for Strength of Concrete*; Bureau of Indian Standards, New Delhi, India, 1959.
52. *RILEM Technical Report 203, Repair Mortars for Historic Masonry. Repair Mortars for Historic Masonry—State of the Art Report of RILEM Technical Committee TC 203-RHM*; Maurenbrecher, P., Groot, G., Eds.; Rilem: Paris, France, 2016; p. 178.
53. RILEM TC 25-PEM, Recommended tests to measure the deterioration of stone to assess the effectiveness of treatment methods. *Mater. Struct.* **1980**, *13*, 175–253.
54. Asadi, I.; Shafigh, P.; Abu Hassan, Z.F.B.; Mahyuddin, N.B. Thermal conductivity of concrete—A review. *J. Bui. Eng.* **2018**, *20*, 81–93.
55. Barbero-Barreraa, M.M.; García-Santos, A.; Neila-González, F.J. Thermal conductivity of lime mortars and calcined diatoms. Parameters influencing their performance and comparison with the traditional lime and mortars containing crushed marble used as renders. *Ener. Buil.* **2014**, *76*, 422–428.
56. Costigan, A.; Pavia, S.; Kinnane, O. An experimental evaluation of prediction models for the mechanical behavior of unreinforced, lime-mortar masonry under compression. *J. Build. Eng.* **2015**, *4*, 283–294.
57. Sinha, D.A. Thermal properties of concrete. Available online: https://www.worldwidejournals.com/paripex/recent_issues_pdf/2014/February/February_2014_1392717710_0c336_27.pdf (accessed on 23 May 2020).
58. Demirboga, R.; Gül, R. The effects of expanded perlite aggregate, silica fume and fly ash on the thermal conductivity of lightweight concrete. *Cem. Con. Res.* **2003**, *33*, 723–727.

59. Xu, S.; Liu, J.; Zeng, Q. Towards better characterizing thermal conductivity of cement-based materials: The effects of interfacial thermal resistance and inclusion size. *Mate. Des.* **2018**, *157*, 105–118.
60. Mnahoncáková, F.; Jiricková, M.; Pavlík, Z.; Fiala, L.; Rovnaníková, P.; Bayer, P.; Cerny, R. Effect of moisture on the thermal conductivity of a cementitious composite. *Int. J. Thermophys.* **2006**, *27*, 1228–1240.
61. Cerny, R.; Drchalová, J.; Kunca, A.; Tydlität, V.; Rovnaníková, P. Thermal and hygric properties of lime plasters with pozzolanic admixtures for historical buildings. In *Research in Building Physics*; Carmeliet, J., Hens, H., Vermeir, G., Eds.; Swets & Zeitlinger: Lisse, Netherlands, 2003; pp. 27–35.
62. Shanmugavel, D.; Thirumalini, S.; Ramadoss, R.; Raneri, S. Interaction of a viscous bio-polymer from green plants with cement paste to produce sustainable concrete; *Constr. Build. Mater.* **2020**, *257*, 119585.
63. Pradeep, S.; Thirumalini, S. Identification of Bio-Minerals and Their Origin in Lime Mortars of Ancient Monument: Thanjavur Palace, *Int. J. Arch. Her. Cons. Rest*. **2019**, doi:10.1080/15583058.2019.1623341.
64. Pradeep, S.; Thirumalini, S. Production of Organic Lime Mortar to Adapt CO2 for Construction of Scared Groves @ Auroville, Puducherry, India. In *Structural Analysis of Historical Constructions*; Aguilar, R., Torrealva, D., Moreira, S., Pando, M., Ramos, L.F., Eds.; RILEM Bookseries: Paris, France, 2018; pp. 2439–2447, doi:10.1007/978-3-319-99441-3_262.
65. Madhavi, T.C.; Annamalai, S. Electrical conductivity of concrete. *ARPN J.* **2016**, *11*, 5979–5982.
66. Tamás, F.D. Electrical conductivity of cement pastes. *Cem. Concr. Res.* **1982**, *12*, 115–120.
67. Spragg, R.; Bu, Y.; Snyder, K.; Bentz, D.; Weiss, J. *Electrical Testing of Cement-Based Materials: Role of Testing Techniques, Sample Conditioning, and Accelerated Curing*; Joint Transportation Research Program: West Lafayette, Indiana, 2013.
68. Liang, K.; Zeng, X.; Zhou, X.; Qu, F.; Wang, P. A new model for the electrical conductivity of cement-based material by considering pore size distribution. *Mag. Concr. Res.* **2017**, *69*, 1067–1078.
69. Morsy, M.S.; Abo El-Enein, S.A.; Hanna, G.B. Microstructure and hydration characteristics of artificial pozzolana-cement pastes containing burnt kaolinite clay. *Cem. Concr. Res.* **1997**, *27*, 1307–1312.
70. Venkatraman, K.; Tamizharasan, V. Electrically Conductive Concrete. *Int. J. Innov. Res. Sci. Eng. Technol.* **2015**, *4*, 6738–6743.
71. Chung, D.D.L. Electrically Conductive Cement-based Materials. *Adv. Cement Res.* **2004**, *16*, 167–176.
72. Olatinsu, O.B.; Olorode, D.O.; Oyedele, K.F. Radio frequency dielectric properties of limestone and sandstone from Ewekoro, Eastern Dahomey Basin. *Adv. Appl. Sci. Res.* **2013**, *4*, 150–158.